

## Model studies of heterogeneous catalytic hydrogenation reactions with gold

Cite this: *Chem. Soc. Rev.*, 2013, **42**, 5002

Ming Pan,<sup>a</sup> Adrian J. Brush,<sup>a</sup> Zachary D. Pozun,<sup>b</sup> Hyung Chul Ham,<sup>a</sup> Wen-Yueh Yu,<sup>a</sup> Graeme Henkelman,<sup>b</sup> Gyeong S. Hwang<sup>a</sup> and C. Buddie Mullins<sup>\*ab</sup>

Supported gold nanoparticles have recently been shown to possess intriguing catalytic activity for hydrogenation reactions, particularly for selective hydrogenation reactions. However, fundamental studies that can provide insight into the reaction mechanisms responsible for this activity have been largely lacking. In this tutorial review, we highlight several recent model experiments and theoretical calculations on a well-structured gold surface that provide some insights. In addition to the behavior of hydrogen on a model gold surface, we review the reactivity of hydrogen on a model gold surface in regards to NO<sub>2</sub> reduction, chemoselective C=O bond hydrogenation, ether formation, and O–H bond dissociation in water and alcohols. Those studies indicate that atomic hydrogen has a weak interaction with gold surfaces which likely plays a key role in the unique hydrogenative chemistry of classical gold catalysts.

Received 21st December 2012

DOI: 10.1039/c3cs35523c

[www.rsc.org/csr](http://www.rsc.org/csr)

### Key learning points

1. Classical supported gold catalysts show high activity for selective hydrogenation reactions but supporting fundamental studies are lacking.
2. H<sub>2</sub> dissociation is a key step for hydrogenation and likely occurs on gold defect sites or the interface between a gold particle and the support on classical gold-based catalysts.
3. H<sub>2</sub> dissociation has a high barrier on Au(111) so atomic hydrogen is used to populate the surface.
4. Atomic hydrogen has a weak interaction with the Au(111) surface with a low desorption activation energy.
5. Several examples are shown that demonstrate the hydrogenation reactivity on Au(111), including NO<sub>2</sub> reduction, C=O group hydrogenation, and the OH + H interaction.

## 1. Introduction

Gold has historically been considered catalytically inert. However, in recent decades, highly dispersed nano-scale gold particles supported on metal oxides have been synthesized and found to exhibit unexpectedly high activity for some chemical reactions. In pioneering work, Haruta discovered that gold nanoparticle catalysts have extraordinary activity for CO oxidation.<sup>1</sup> This work prompted numerous follow up studies, and to date, gold-based heterogeneous catalysts have shown a high activity for many oxidation reactions.<sup>2</sup> Related fundamental studies have also been extensively conducted both experimentally<sup>3,4</sup> and theoretically.<sup>5</sup>

Additionally, gold-based catalysts have also been studied in hydrogenation reactions. Bond *et al.* employed supported gold catalysts for selective hydrogenation of 1,3-butadiene<sup>6</sup> and later Hutchings *et al.* studied hydrochlorination of acetylene<sup>7</sup> over gold. To date, many studies have been conducted for several other hydrogenation reactions on gold-based catalysts as well.<sup>8,9</sup> However, few fundamental studies on model gold surfaces have been performed.<sup>10,11</sup> In this review article, we will summarize and discuss the current progress on fundamentals of hydrogenation chemistry of gold with an emphasis on experiments conducted on gold single crystals in vacuum.<sup>12–17</sup>

### 1.1 Advances in hydrogenation reactions with classical gold catalysts

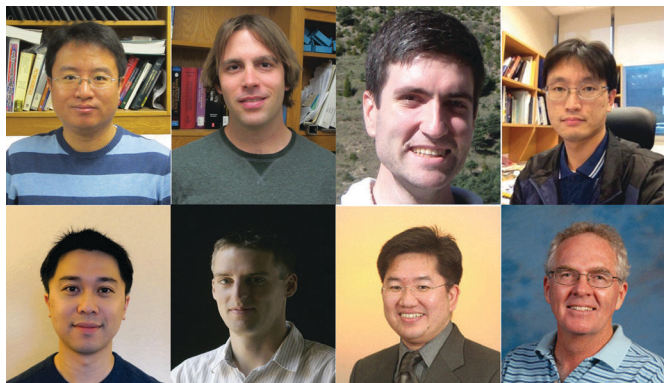
Gold can be used as a catalyst for hydrogenation of various hydrocarbons with one or more unsaturated bonds (*i.e.* C=C, C≡C, C=O, and C≡O), such as CO,<sup>18</sup> CO<sub>2</sub>,<sup>19</sup> acyclic alkenes,<sup>20</sup> cyclic alkenes,<sup>21</sup> alkynes,<sup>22</sup> derivatives of benzene,<sup>23</sup> and unsaturated aldehydes.<sup>24</sup> In particular, gold-based catalysts

<sup>a</sup> Department of Chemical Engineering, University of Texas at Austin, Austin, TX 78712-0231, USA. E-mail: [mullins@che.utexas.edu](mailto:mullins@che.utexas.edu); Fax: +1 512-471-7060; Tel: +1 512-471-5817

<sup>b</sup> Department of Chemistry and Biochemistry, University of Texas at Austin, Austin, TX 78712, USA

show great promise in applications for selective hydrogenation processes. Three of the most prominent examples are: (1) selective hydrogenation of acetylene to ethylene with a selectivity higher than 90%;<sup>25</sup> (2) chemoselective hydrogenation of unsaturated aldehydes (such as acrolein) to yield unsaturated alcohols with 10 times higher selectivity than traditional platinum-based catalysts;<sup>26</sup> and (3) for nitro-unsaturated molecules, NO<sub>2</sub> groups have a high chemoselectivity (>95%) compared to other unsaturated functional groups present on the molecule, such as C=C, C=O, C≡N, and benzene groups.<sup>27</sup>

Gold-based catalysts show intriguing activity for hydrogenation reactions. We speculate that a single H atom is likely one of the more active species on gold surfaces since it is very weakly bound. This phenomenon is likely similar to the observations of O on gold: model studies indicate that oxygen atoms have a weaker interaction with Au surfaces compared to other metallic surfaces, leading to extraordinary activity for selective oxidation reactions.<sup>28</sup> Thus, in order to verify this speculation and explore the related reaction mechanisms, fundamental studies of hydrogenation transformations with H on Au surfaces are needed.



(From left to right, top row) Ming Pan, Adrian J. Brush, Zachary D. Pozun, Hyung Chul Ham, (bottom row) Wen-Yueh Yu, Graeme Henkelman, Gyeong S. Hwang, C. Buddie Mullins

Ming Pan completed his BS and MS at Tianjin University, China and a second MS in Chemical Engineering at Tufts University. Currently, Ming is a PhD graduate student in the Mullins research group in the Department of Chemical Engineering at the University of Texas at Austin. Ming previously held the William S. Livingston Fellowship from the graduate school at UT Austin. His research focuses on fundamental studies of heterogeneous catalysis on gold and iridium model surfaces. This work aims to provide insights into reaction mechanisms and enhance better understanding of activity of classical supported catalysts. Adrian completed his BS in Chemical Engineering from UC Berkeley in 2008. He spent 2.5 years working as an R+D Process Development Engineer at The Clorox Company and 6 months as a Senior Research Associate at Lawrence Berkeley National Laboratory before starting his pursuit of a PhD in Chemical Engineering with the Mullins group at the University of Texas at Austin. He is currently researching catalysis and surface science in order to better understand heterogeneously catalyzed reaction mechanisms.

Zachary D. Pozun received a BS from the University of Pittsburgh in 2007 while conducting research at the NASA-Goddard Space Flight Center. He received his PhD in 2012 from the University of Texas at Austin under the direction of Prof. Graeme Henkelman and investigated the properties of nanomaterials for applications in catalysis and separations. He is currently an NSF CI TraCS postdoctoral fellow with Prof. Kenneth Jordan at Pittsburgh and is applying quantum Monte Carlo methods to realistic material systems.

Dr Ham is currently a senior research staff scientist in the Fuel Cell Research Center at the Korea Institute of Science and Technology (KIST) Seoul. His main research interest is the rational design of nanocatalysts for energy conversion and storage (fuel cells, supercapacitors and photovoltaics) using the combined first-principles density functional calculation and experimental method. After working at KIST as a research staff scientist, he pursued and gained a PhD degree in chemical engineering from the University of Texas at Austin in 2011 under the guidance of Prof. Gyeong S. Hwang.

Wen-Yueh Yu received his BS and MS in Chemical Engineering from National Taiwan University in Taiwan. After working as a research assistant in the Institute of Chemistry at Academia Sinica in Taiwan, he came to the University of Texas at Austin to pursue his PhD in Chemical Engineering under the supervision of Professor C. Buddie Mullins. His research interests lie in catalyst chemistry, surface science and nanotechnology with particular interests in their application to renewable energy. Currently he is studying the catalytic chemistry on Pd–Au bimetallic model surfaces with the aim of molecular-level understanding.

Professor Graeme Henkelman obtained his PhD in Chemistry at the University of Washington at Seattle. After postdoctoral studies at Los Alamos National Laboratory he joined the University of Texas at Austin where he is currently an Associate Professor of Chemistry. His research group focuses on the development of new computational algorithms for finding chemical reaction pathways and extending the time scale of simulations beyond what can be simulated directly with molecular dynamics. These methods allow for the investigation of reactions at surfaces, novel catalysts, defect dynamics in materials, and new battery materials.

Professor Gyeong S. Hwang obtained his PhD in Chemical Engineering at the California Institute of Technology. After postdoctoral stints at the Max Planck Institute for Solid State Research in Stuttgart, Germany and at Caltech he joined the University of Texas at Austin where he is a Professor of Chemical Engineering and he holds the Lyondell Chemical Company Endowed Faculty Fellowship. His research group focuses on the development of first principles-based multiscale computational schemes that allow for the systematic investigation of the synthesis and structure–property relationships of various nanostructured materials for energy and electronics applications.

Professor C. Buddie Mullins attended the California Institute of Technology to obtain a PhD in Chemical Engineering and then joined the IBM Almaden Research Center as a visiting scientist for two years. He joined UT-Austin in 1991 and is currently a Professor of Chemical Engineering and Chemistry and he holds the Z. D. Bonner Professorship. His group is interested in advanced materials for lithium-ion batteries, photomaterials and strategies for solar photoelectrochemistry, and surface chemistry/catalysis.

## 1.2 H<sub>2</sub> dissociation on gold catalysts

Generally, H<sub>2</sub> dissociation has been considered as a key step in hydrogenation reactions. Norskov and coworkers conducted density functional theory (DFT) calculations and predicted that H<sub>2</sub> dissociation has a high energetic barrier and is activated on a Au(111) surface.<sup>29</sup> However, for classical gold catalysts, H<sub>2</sub> dissociation likely occurs at low-coordinated sites and/or the interface between the gold particles and the metal oxide support. Fujitani and coworkers observed H–D production from H<sub>2</sub> and D<sub>2</sub> by using two types of model catalysts – Au/TiO<sub>2</sub>(110)<sup>10</sup> and TiO<sub>2</sub>/Au(111),<sup>30</sup> and they provided evidence that H<sub>2</sub> dissociation occurs at the interface of the gold particles and TiO<sub>2</sub>. However, Yates and Morris employed transmission Fourier transform infrared (FTIR) spectroscopy and CO oxidation as a probe reaction to demonstrate that the most active sites for hydrogen dissociation on Au/TiO<sub>2</sub> are the free step edges or other defect sites on Au particles.<sup>31</sup> Additionally, they found that dissociated atomic H can diffuse to the TiO<sub>2</sub> support, possibly *via* spillover onto the flat Au faces.<sup>31</sup> Therefore, we speculate that after H<sub>2</sub> dissociation on defect or interface sites, the subsequent hydrogen atoms will “spill over” onto the predominantly Au(111) face of the gold particle, and these activated hydrogen atoms are the reactive species for some hydrogenation reactions occurring on gold catalysts. Thus, in order to conduct fundamental studies regarding hydrogenation on a model gold surface such as Au(111), it is necessary to populate the surface with atomic hydrogen to simulate H<sub>2</sub> dissociation and spillover onto the surface.

However, whether H atoms can spillover/diffuse onto other portions of the gold surface after dissociating on active sites, such as low-coordinated gold sites and interfaces, is still an open question. In addition to the Yates and Morris research,<sup>31</sup> Bron and coworkers studied hydrogenation of acrolein on Ag high-surface-area catalysts and suggested that H<sub>2</sub> dissociates on defect sites on silver particles and spills over onto the face sites.<sup>32</sup> Since H atoms have similar binding energies on Ag(111) and Au(111) based on DFT calculations<sup>33</sup> and TPD (temperature programmed desorption) measurements,<sup>13,34</sup> it is reasonable to speculate that H atoms might also be able to diffuse onto gold face sites after H<sub>2</sub> dissociation at a defect or interface site. If hydrogen atoms are able to spill over onto the flat Au surface, these hydrogen atoms likely contribute significantly to the reactivity for hydrogenation reactions on gold.

Sykes and coworkers addressed this issue employing scanning tunneling microscopy (STM) to study H<sub>2</sub> adsorption on Pd/Au(111).<sup>35</sup> They exposed the sample to H<sub>2</sub> at 420 K and then cooled it to 7 K, after which they did not detect any H atoms on the Au surface *via* STM. They suggested that H atoms cannot diffuse onto the Au(111) surface from the Pd–Au interfaces due to the strong binding energy at the interface. However, since they exposed the Au(111) sample to H<sub>2</sub> at 420 K,<sup>35</sup> it cannot be ruled out that the generated H atoms did diffuse on to the Au(111) surface, but then immediately recombined to desorb from the surface at this elevated temperature. Similarly, Bus and coworkers studied H<sub>2</sub> dissociation on Al<sub>2</sub>O<sub>3</sub>-supported gold catalysts and also suggested that the generated H atoms cannot diffuse onto gold face sites.<sup>36</sup> Using EXAFS (extended X-ray adsorption fine structure) techniques to estimate Au particle size and number of surface Au atoms, they estimated the ratio of H to surface Au atoms during hydrogen chemisorption to be lower

than 100%, and increases with reducing gold particle size, suggesting H atoms do not bind to all the exposed sites on gold particles and likely adsorb only on the low coordinated sites that they dissociated on, such as edges and corners.<sup>36</sup> However, the catalysts were tested at 298 K or higher temperatures, which again likely causes immediate H<sub>2</sub> recombinative desorption after diffusing onto the face sites. While the authors of both of these studies suggest that hydrogen atoms do not spillover, neither of the above two studies can definitively disprove the ability for hydrogen atoms to “spill over” onto gold surfaces.

Since active hydrogenation chemistry has been observed classically on supported gold catalysts, we have conducted studies regarding hydrogenation reactions on a Au(111) model surface in order to better understand the role of gold in hydrogenation transformations on classical Au-based catalysts and to provide insights into the reaction mechanisms.

## 2. H on a model gold surface

Since hydrogen has a large barrier to dissociatively adsorb on model gold surfaces,<sup>29</sup> atomic hydrogen is necessary for populating H atoms on the surface in vacuum in order to study hydrogenation reactions. Sault and coworkers populated the surface of a Au(110)-(1 × 2) sample by exposing it to H<sub>2</sub> with their QMS (quadrupole mass spectrometer) filament turned on. Their TPD measurements showed a hydrogen desorption feature at ~216 K (Fig. 1a, black curve).<sup>11</sup>

Recently, our group employed an electron-beam heated thermal H-atom generator to adsorb atomic hydrogen on Au(111) at 77 K with subsequent TPD measurements.<sup>13</sup> The green curve in Fig. 1a illustrates TPD from the sample surface saturated by H atoms, which we define as unity relative coverage,  $\theta_{\text{H,rel}} = 1$ , (we are unsure of the exact ratio of H atoms to Au atoms). The recombinative H<sub>2</sub> desorption shown in this experiment yields a single feature with the peak temperature at ~111 K, indicating a low desorption activation energy and suggesting a weak interaction between atomic H and the Au(111) surface. With changing coverages of H atoms, the desorption feature shows approximately similar peak temperatures over a narrow range of 108–111 K, suggesting that H<sub>2</sub> recombinative desorption on Au(111) follows first-order desorption kinetics. This is a deviation from most other examples of recombinative desorption, which typically display second-order kinetics. We can estimate the desorption activation energy based on the Redhead approximation with a frequency factor of  $10^{13} \text{ s}^{-1}$ . Using 110 K for the peak temperature, the desorption activation energy for H<sub>2</sub> is estimated to be ~28 kJ mol<sup>-1</sup> (0.29 eV).<sup>13</sup> Since the recombination and desorption of H<sub>2</sub> includes the formation of a H–H bond, the H–H bond energy for gaseous molecular hydrogen (DE), the H–Au binding energy (BE), and H<sub>2</sub> desorption activation energy ( $\Delta E_{\text{d}}$ )<sup>33</sup> are all related by the equation:  $2\text{BE} = \text{DE} + \Delta E_{\text{d}}$ . Using 28 kJ mol<sup>-1</sup> (0.29 eV) for the desorption activation energy and 436 kJ mol<sup>-1</sup> (4.52 eV) for the H–H bond energy, the binding energy between the H atom and the Au(111) surface is estimated to be ~232 kJ mol<sup>-1</sup> (2.40 eV), which is in good agreement with DFT calculations done by Greeley and Mavrikakis (2.22 eV).<sup>33</sup>

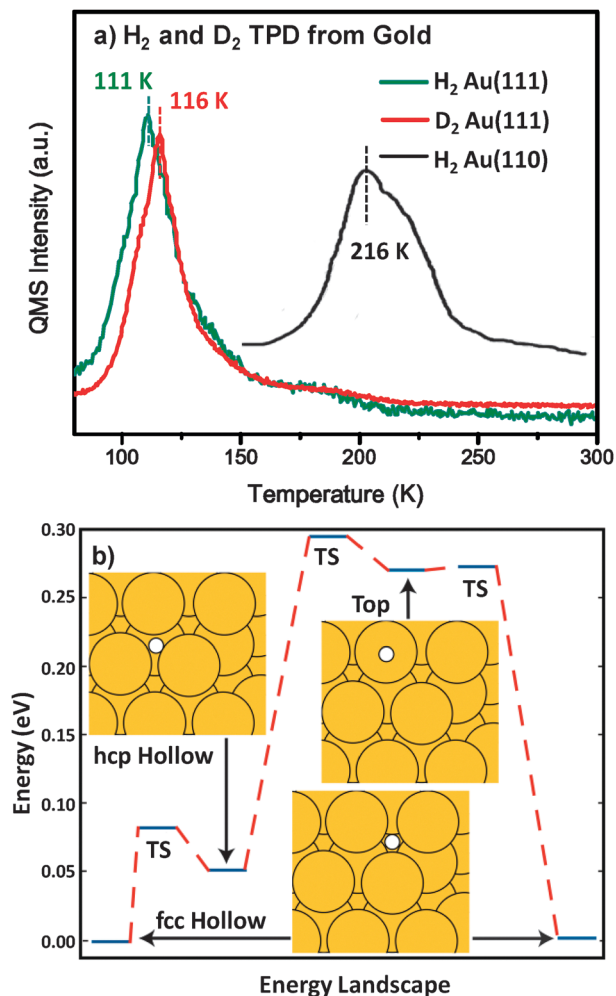


**Fig. 1** (a) H<sub>2</sub> ( $\theta_{\text{H,rel}} = 1$ ) and D<sub>2</sub> ( $\theta_{\text{D,rel}} = 0.8$ ) TPD from H and D atom covered Au(111). The black curve indicates H<sub>2</sub> desorption from the Au(110) surface (adapted from Sault *et al.*<sup>11</sup>). (b) Schematic mechanisms of the diffusion of an H atom on Au(111).<sup>16</sup> All figures obtained with permission. Copyright (2012) American Chemical Society.

In addition, Fig. 1a illustrates that D<sub>2</sub> yields a desorption feature at slightly higher temperature, 116 K, indicative of a higher desorption activation energy ( $\sim 30 \text{ kJ mol}^{-1}$ ). This phenomenon likely stems from the lower zero point energy of D<sub>2</sub> compared to H<sub>2</sub>, leading to a stronger binding energy with the Au(111) surface. This property can cause kinetic isotope effects (KIE)<sup>48</sup> where H (or compound X–H) has higher reactivity than D (or X–D). To further understand the mechanisms and energetics involved in this hydrogen recombinative desorption process, we performed DFT calculations, as shown in Fig. 1b. These calculations indicate that H atoms favor adsorbing on fcc hollow sites and have a small barrier of 0.07 eV to diffuse to hcp hollow sites, suggesting that H atoms can move around on the surface, even at a low temperatures such as 77 K.<sup>16</sup> For H to recombinatively desorb or participate in other chemical reactions, H atoms need to diffuse onto the atop sites of Au(111) with a barrier of 0.30 eV.<sup>16</sup> This is also consistent with our TPD measurements<sup>13</sup> and computational results conducted by Mavrikakis.<sup>33</sup>

However, H<sub>2</sub> desorption temperatures can vary widely between the different faces of the same metal. For example, the H<sub>2</sub> desorption temperature from Au(111) is much lower than the peak temperature from Au(110) at 216 K, indicating a higher desorption activation energy on Au(110) of  $\sim 51 \text{ kJ mol}^{-1}$ .<sup>11</sup> This comparison clearly demonstrates that the surface structure can significantly affect H desorption from gold. Further, the kind of metal and its various surface structures are closely associated with its catalytic properties and play a key role in determining the surface chemistry for chemical reactions. Therefore, it is educational to examine the peak desorption temperatures, as shown in Table 1, for H<sub>2</sub> desorption from a variety of metal surfaces. The desorption temperatures suggest the binding energy of H on these various metal surfaces increases roughly in the order of Au < Ag < Cu, Al, Ni, Pd, Pt, Ir, Ru < Mo, W, Fe. From DFT calculations,<sup>33</sup> H atoms have a small binding energy on Ag(111), Au(111), and Cu(111). This is consistent with the TPD measurements, in which a measurable amount of H<sub>2</sub> does not dissociatively adsorb on those surfaces and atomic hydrogen has been employed, as shown in the “Hydrogen Source” column in Table 1. However, it should be noted that the H<sub>2</sub> desorption temperature on Cu(111) is much higher than that on Au and Ag.

There are multiple desorption features on some metallic surfaces. The authors reporting these results speculate in their papers that the low temperature peaks are due to subsurface H desorption from H atoms that diffuse into the bulk. These sub-surface H features appear with increasing coverage of hydrogen on the surface and can even be larger than the saturated surface H desorption feature. Note that two peaks are observed for subsurface H desorption on Ag(100) at 110 and 120 K, possibly due to surface reconstruction during the adsorption of H.<sup>34</sup> In addition, on many metal surfaces such as Pd, Ir, Pt, W, Ru, and Mo, molecular hydrogen dissociatively adsorbs on the surface frequently leading to second-order kinetics for the recombinative desorption rate, which results

**Table 1** Desorption of H<sub>2</sub> on transition metal surfaces

Metal surfaces	Hydrogen source	Desorption peak temperatures (K)	Desorption activation energy (eV)	Ref.
Au(111)	Atomic	111	0.29	13
Au(110)	Atomic	216	0.53	11
Ag(111)	Atomic	160	Not reported	34
Ag(100)	Atomic	110, 120, 150	Not reported	34
Cu(111) (D) <sup>a</sup>	Atomic	350	0.78	37
Al(100)	Atomic	310–340	0.76	38
Ni(111)	Molecular	310, 380	1.00	39
Ni(100)	Molecular	360–400	1.00	39
Ni(110)	Molecular	350	0.93	39
Pd(111)	Molecular	205, 280–310	Not reported	40
Ir(111)	Molecular	270–380	0.55	41
Ir(110)	Molecular	200–300, 400	1.00	42
Pt(111)	Molecular	280–350	0.74–0.87	43
Ru(001)	Molecular	320–420	Not reported	44
Mo(110)	Molecular	500–650	1.2–1.5	45
W(110)	Molecular	440–510	1.26–1.52	46
Fe(110) (D) <sup>a</sup>	Molecular	450	Not reported	47

<sup>a</sup> Deuterium is employed in TPD measurements.

in the peak temperature shifting from high temperatures to low temperatures with increasing coverages. Therefore, Table 1 provides a temperature range for H<sub>2</sub> desorption from those surfaces.

### 3. Hydrogenation on Au(111)

H atoms recombinatively desorb from the Au(111) surface at temperatures lower than 160 K as shown in Fig. 1a, providing a small temperature window for testing chemical reactions in vacuum. As such, while we have successfully demonstrated several hydrogenation reactions that occur on Au(111), we have also been unsuccessful in some of our attempts to catalyze a hydrogenation reaction on the Au(111) surface. Table 2 lists experiments that we have examined on the Au(111) surface but for which no reactivity has been detected.

No measurable activity can be the result of a couple different scenarios. First of all, the hydrogen atoms and/or the other reactant(s) are weakly bound to the surface, and could desorb off the surface at temperatures lower than that required to drive the chemical reaction. While this is a limitation in the model experiments, it does not disprove the ability for gold to catalyze a particular reaction. At ambient temperatures and pressures associated with classical gold catalysts, the large number of collisions can result in temporarily adsorbed species with enough energy to drive the reaction. Secondly, the reaction may not occur on the Au(111) surface alone, and may require a low-coordination site, such as a step or edge, or an interface between the gold and the metal oxide. For these reactions, performing experiments on other faces, such as Au(110), or gold/support samples, such as TiO<sub>2</sub>/Au(111) or Au/TiO<sub>2</sub>(110), can illuminate the requirements for a reaction to progress. Combining the knowledge from all of these “puzzle piece” model experiments allows one to better see a complete picture of the classical catalyst.

#### 3.1 NO<sub>2</sub> reduction on H/Au(111)

One of our first successful hydrogenation experiments involved the ability for an H-covered Au(111) surface to reduce NO<sub>2</sub> to NO. It turns out that we employ a NO<sub>2</sub> molecular beam in order to remove contaminants from the Au(111) surface held at 800 K

for cleaning.<sup>13,15</sup> Since NO<sub>2</sub> obviously decomposes on the surface at high temperatures, producing atomic oxygen that can react with carbon contaminants, this indicated that NO<sub>2</sub> has a certain degree of reactivity on the surface that was worth studying with a hydrogen covered Au(111) surface. Additionally, NO<sub>x</sub> (NO<sub>2</sub> and NO) reduction is an important reaction for emission control from automobiles and power plants. Accordingly, gold-based catalysts have been widely studied for NO<sub>x</sub> reduction with H<sub>2</sub> as a reducing agent<sup>49</sup> but the mechanism is not well understood.

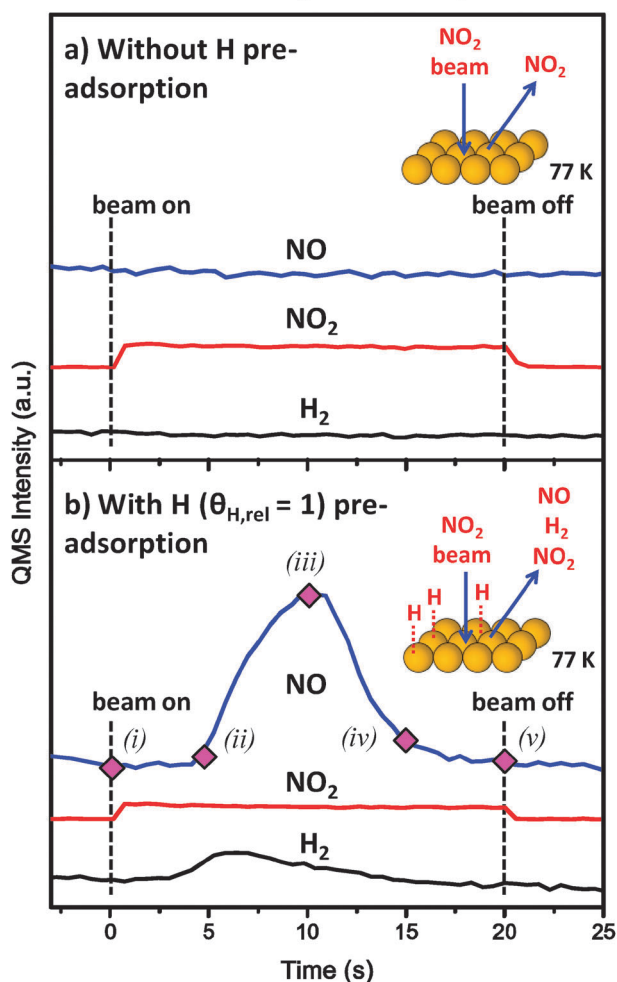
We conducted molecular beam reactive scattering (MBRS) experiments by delivering a NO<sub>2</sub> beam (the kinetic energy is ~0.1 eV) onto H/Au(111) at 77 K.<sup>14</sup> During this process, the species desorbing from the surface can be detected by a quadrupole mass spectrometer to enable the qualitative and quantitative analysis of possible chemical reactions. Fig. 2a illustrates a control experiment by impinging the NO<sub>2</sub> beam onto the clean Au(111) surface without the co-adsorption of H atoms. At  $t = 0$  s for beam-on, the increase of the NO<sub>2</sub> signal is due to a portion of NO<sub>2</sub> molecules scattering off the surface rather than adsorbing (the NO<sub>2</sub> sticking probability on Au(111) is ~60%). During the entire period of the impingement, the NO<sub>2</sub> signal remains a constant and no NO or H<sub>2</sub> are detected, suggesting no reaction occurred on the surface. In contrast, on H-atom covered Au(111), as shown in Fig. 2b, as the NO<sub>2</sub> beam strikes the surface over the 20 second exposure, the NO signal shows an induction period in which there is no NO evolution from  $t = 0$  to 5 seconds, followed by significant NO evolution, suggesting a reaction between NO<sub>2</sub> and H atoms. This process has been divided into 5 reaction stages, labeled as: (i) beam on, (ii) the beginning of NO evolution, (iii) the peak, (iv) the end of NO evolution, and (v) beam off. In addition, our QMS detected H<sub>2</sub> evolution during NO<sub>2</sub> impingement. Note that these phenomena have been observed at a cryogenic temperature of 77 K, indicating a facile reaction and high reactivity for NO<sub>2</sub> on H/Au(111). In experiments exploring only the induction period, the subsequent TPD measurement results show no NO<sub>2</sub> desorption upon heating the surface. Only NO was observed but not any other possible reduced products such as N<sub>2</sub>, N<sub>2</sub>O, and NH<sub>3</sub>, suggesting that NO<sub>2</sub> is completely converted to NO with a 100% conversion and 100% selectivity.<sup>14</sup>

We conducted DFT calculations to explore the reaction mechanisms, which, combined with TPD studies, suggest two intermediates (HNO<sub>2</sub> and N<sub>2</sub>O<sub>3</sub>) for this reaction.<sup>14</sup> The detailed results are shown in Table 3, organized by the experimental stages and H coverages. These results indicate the energy barrier for NO<sub>2</sub> reduction is closely correlated to H coverage – high hydrogen concentration on the surface can enhance the reaction between H and NO<sub>2</sub> to form an HNO<sub>2</sub> intermediate; in contrast, low H coverage (more empty sites) favors the hydrogenation of HNO<sub>2</sub> to produce NO, that can then evolve from Au(111). Thus, NO<sub>2</sub> reduction and NO evolution at 77 K follow a reaction route with the lowest energetic barriers as illustrated by the highlighted elementary steps in Table 3. The induction period (i)–(ii) is due to HNO<sub>2</sub> formation, which is favorable with high H coverage ( $E_a = 0.04$  eV, compared to

**Table 2** Experiments on H/Au(111) not showing hydrogenative reactivity

Reactant on H/Au(111)	Desorption temperature on clean Au(111) (K)
CO	90
CO <sub>2</sub>	90
C <sub>2</sub> H <sub>4</sub>	90
NO	90
N <sub>2</sub> O	90
CH <sub>2</sub> =CH-CHO	160 <sup>a,b</sup>
CH <sub>3</sub> CH <sub>2</sub> CH <sub>2</sub> CH <sub>2</sub> C≡CH	210 <sup>b</sup>
CH <sub>3</sub> CH <sub>3</sub> CH=CH-CHO	210 <sup>b</sup>
CH <sub>3</sub> CH <sub>2</sub> CH <sub>2</sub> -NO <sub>2</sub>	200 <sup>b</sup>

<sup>a</sup> The reaction can be detected but the reactivity is very small. <sup>b</sup> The temperature is the peak of monolayer desorption.

20s (2.0 ML) NO<sub>2</sub>/Au(111), T<sub>s</sub> = 77 K

**Fig. 2** NO<sub>2</sub> reduction and NO evolution from H covered Au(111) in molecular beam reactive scattering experiments. The beam strikes onto (a) the clean Au(111) surface (b) the H (relative coverage  $\theta_{\text{H,rel}} = 1$ ) atom pre-covered Au(111) surface at 77 K. The NO<sub>2</sub> beam was impinging on the surface from 0 s to 20 s. The points denoted (i)–(v) mark specific times corresponding to measurements discussed in the paper. The beam flux is 0.1 monolayer per s. Note that (a) and (b) have the same Y-axis scale.<sup>14</sup> All figures obtained with permission. Copyright (2012) American Chemical Society.

$E_a = 0.55$  eV at  $\theta_{\text{H}} \sim 0$ ). In contrast, HNO<sub>2</sub> hydrogenation and NO production, steps (ii)–(iv), have a lower barrier with low H coverage. Thus, HNO<sub>2</sub> formation creates more empty sites on the surface that promotes further HNO<sub>2</sub> hydrogenation, which is highly exothermic (0.9 eV) and likely causes NO evolution at 77 K. The second intermediate, N<sub>2</sub>O<sub>3</sub>, is due to the reaction between adsorbed NO<sub>2</sub> and surface NO produced from reaction. We interpret the desorption of both NO and NO<sub>2</sub> from TPD measurements following 10 seconds of NO<sub>2</sub> impingement on H/Au(111), denoted by point (iii), as decomposition products of this intermediate. Reflection-absorption infrared spectroscopy (RAIRS) also gives evidence for two intermediates, indicated by the appearance of a new feature with H co-adsorption on Au(111). This feature shifts with reaction progress, indicating the transformation from one intermediate to the other, likely

**Table 3** Energetics/barriers of surface reactions during MBRS experiments.<sup>14</sup> Copyright (2012) American Chemical Society

Reaction	$\theta_{\text{H}} \sim 1 (\theta_{\text{E}} \sim 0)$		$\theta_{\text{H}} \sim 0 (\theta_{\text{E}} \sim 1)$	
	$\Delta E$ (eV)	$E_a$ (eV)	$\Delta E$ (eV)	$E_a$ (eV)
(i) and (ii) Induction				
NO <sub>2</sub> (g) → NO <sub>2</sub>	−0.30		−0.81	
NO <sub>2</sub> + H → H <sub>dw</sub> ONO	−1.13	0.04	−0.45	0.55
H <sub>dw</sub> ONO → H <sub>up</sub> ONO <sup>a</sup>	−0.02	0.28	−0.24	0.35
(ii)–(iv) NO evolution				
H + H <sub>up</sub> ONO → NO + H <sub>2</sub> O	−0.72	0.47	−0.90	0.30
NO + NO <sub>2</sub> → N <sub>2</sub> O <sub>3</sub>			−0.03	0.27
(iv) and (v) Post-evolution				
NO <sub>2</sub> (g) → NO <sub>2</sub>			−0.81	

<sup>a</sup> Note that HNO<sub>2</sub> undertakes a transformation for adsorption states from H<sub>dw</sub>NO<sub>2</sub> and H<sub>up</sub>NO<sub>2</sub>, respectively regarding hydrogen face-down and face-up configurations.

HNO<sub>2</sub> to N<sub>2</sub>O<sub>3</sub>. Finally, we note that the formation of HNO<sub>2</sub> is a highly exothermic process (1.13 eV), which likely leads H<sub>2</sub> to desorb from the surface at 77 K.<sup>14</sup>

### 3.2 C=O group hydrogenation on H/Au(111)

Gold-based catalysts have been identified with high activity for selective hydrogenation of unsaturated aldehydes to unsaturated alcohols.<sup>26</sup> In this reaction, the C=C group is thermodynamically more favorable for hydrogenation than the C=O bond. Interestingly, gold catalysts can yield a selectivity of 60% for unsaturated alcohols.<sup>8</sup> Thus, fundamental studies are needed for a better understanding of the reaction mechanisms. We conducted experiments with acrolein on H covered Au(111) as mentioned in Table 2. However, the product signals are very small and it is difficult to interpret the experimental results. Therefore, we employed compounds only containing a C=O bond (such as aldehydes and ketones) to perform a model hydrogenation reaction on Au(111) in order to access the mechanistic information.

**3.2.1. Chemoselective hydrogenation of aldehydes and ketones.** We first studied acetaldehyde on H-covered Au(111) and observed the production of ethanol.<sup>13</sup> This hydrogenation reaction can be considered as a probe reaction demonstrating the surface chemistry of Au(111) for C=O hydrogenation. This study demonstrates that acetaldehyde can be hydrogenated to ethanol at temperatures lower than ~250 K and that hydrogenation with D atoms exhibits much lower activity than with H atoms, indicative of a kinetic isotope effect.

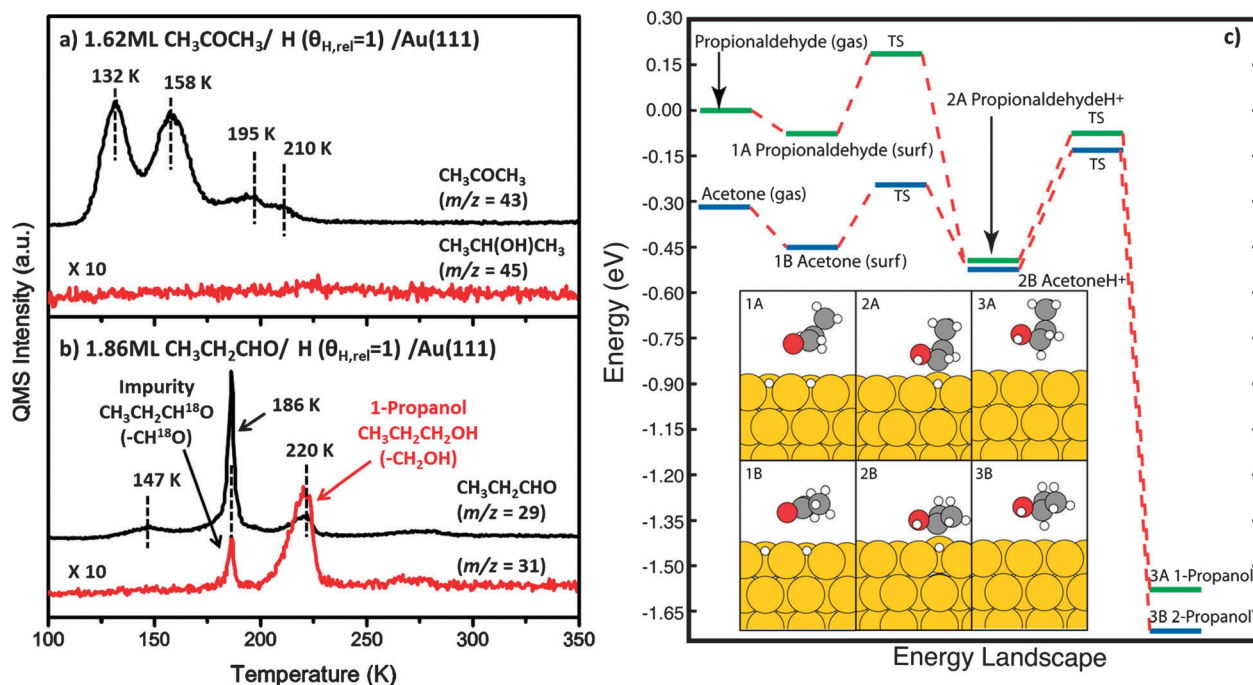
In order to access more information regarding C=O hydrogenation reactions in gold catalysis, we compared the hydrogenation reactivity of acetone and propionaldehyde, two isomers with the C=O bond located on the middle and terminal carbon atom, respectively. On a clean Au(111) surface, acetone has three desorption features at 130 K, 132 K, and 155 K, responsible for the desorption of multilayer, second-layer, and monolayer, respectively, in agreement with the result previously reported by Syomin and Koel.<sup>50</sup> Acetone also shows a noticeable interaction with H adatoms on Au(111).

Fig. 3a shows TPD spectra of acetone and 2-propanol (the product of acetone hydrogenation) from 1.62 ML (monolayer) of acetone adsorbed on Au(111) with pre-adsorption of H atoms ( $\theta_{\text{H,rel}} = 1$ ), displaying several changes in the acetone spectrum compared to the control experiment – the desorption features from the second-layer and monolayer are broader and the monolayer feature shifts to a slightly higher temperature, 158 K; in addition, two new desorption features appear at higher temperatures (195 and 210 K). These results suggest an interaction between H and acetone. However, no hydrogenated products such as 2-propanol, were observed, indicative of immeasurable reactivity of acetone for hydrogenation reactions on Au(111).<sup>15</sup>

In contrast, propionaldehyde is observed to be hydrogenated to 1-propanol as shown in Fig. 3b, in which 1.86 ML propionaldehyde is adsorbed on H covered ( $\theta_{\text{H,rel}} = 1$ ) Au(111). On the clean Au(111) surface, 1.86 ML of propionaldehyde yields three desorption features at 121 K, 154 K, and 269 K, respectively for multilayer, monolayer, and polymer desorption. Here, the polymerization of aldehyde was also observed for acetaldehyde on Au(111) and has been reported on other metal surfaces.<sup>13</sup> However, on the H covered Au(111) surface as shown in Fig. 3b, the TPD spectrum of propionaldehyde, indicated by  $m/z = 29$ , shows a complicated transformation indicative of a strong interaction between propionaldehyde and H adatoms. In addition, the spectrum for  $m/z = 31$  has a desorption feature at 220 K, which indicates the formation of 1-propanol. The other features are due to a mass fragment of propionaldehyde. We estimate that 90% of the desorption peak at 220 K results from the desorption of 1-propanol. We also studied the

hydrogenation of propionaldehyde on deuterium-covered Au(111) and detected the formation of deuterated 1-propanol ( $\text{CH}_3\text{CH}_2\text{CHDOD}$ ) indicated by a single desorption feature for the characteristic mass fragment of 33 ( $-\text{CHDOD}$ ) at 220 K, clearly suggesting the formation of 1-propanol from hydrogenation of propionaldehyde on Au(111).<sup>15</sup>

Based on the discussion above, it is clear that acetone and propionaldehyde have significantly different reactivities for hydrogenation with H atoms on Au(111) – propionaldehyde can be reduced to 1-propanol but acetone cannot be hydrogenated. This can be attributed to different energetic barriers as shown in Fig. 3c. Ketones have lower thermodynamic stability compared to aldehydes, therefore, our DFT calculations indicate that acetone is 0.33 eV lower in energy than propionaldehyde in the gas phase. Both of them have a low binding energy of  $\sim 0.1$  eV with the Au(111) surface and need to overcome a similar barrier of 0.2 eV for the first hydrogenation step on the carbonyl oxygen. Following that, the carbonyl carbon forms a covalent bond with the surface and is vulnerable to attack by surface hydrogen atoms. When the second hydrogen attacks the  $\alpha$  carbon, propionaldehyde has a high reverse reaction energy barrier and favors hydrogenation to 1-propanol. Conversely, acetone has a higher barrier to convert to 2-propanol compared to the reverse reaction, leading to a low reactivity. Another key factor is due to polymerization of propionaldehyde, which was observed on Au(111) and causes the desorption of propionaldehyde at higher temperatures. Our DFT calculations predict that H adatoms can promote this polymerization of propionaldehyde, which allows propionaldehyde to remain on the surface at a higher temperature, increasing the reaction probability.<sup>15</sup>



**Fig. 3** (a) Acetone hydrogenation on H covered Au(111). (b) Propionaldehyde hydrogenation on H/Au(111). (c) Energy diagram for acetone and propionaldehyde hydrogenation on Au(111).<sup>15</sup> All figures obtained with permission. Copyright (2012) John Wiley and Sons.

**3.2.2. Reductive ether synthesis *via* coupling of aldehydes and alcohols.** When we studied the hydrogenation of acetaldehyde and propionaldehyde on H/Au(111), we observed another reaction channel leading to the production of symmetrical diethyl ether and di-*n*-propyl ether, respectively.<sup>12</sup> In addition, water has also been detected during these reactions, suggesting the reductive self-coupling reactions of:  $2\text{H} + 2\text{CH}_3\text{CHO} \rightarrow (\text{CH}_3\text{CH}_2)_2\text{O} + \text{H}_2\text{O}$  and  $2\text{H} + 2\text{CH}_3\text{CH}_2\text{CHO} \rightarrow (\text{CH}_3\text{CH}_2\text{CH}_2)_2\text{O} + \text{H}_2\text{O}$ , as shown in Fig. 4.<sup>12</sup>

These results represent an alternative method to synthesize ethers. Currently, there are two methods commonly used for ether synthesis.<sup>51</sup> One is the reaction of alcohols and mineral acids. However, this reaction must be operated at harsh conditions with high temperature and a strong acid, leading to undesired byproducts, such as olefins *via* acid-mediated dehydration. The other reaction is the Williamson method, which can present environmental and capital issues since toxic and expensive alkyl halides are used.<sup>51</sup> The method for ether production with an aldehyde self-coupling reaction has been reported by Milone and coworkers.<sup>52</sup> They produced cinnamyl ethyl ether and 2-ethoxyprop-1-enylbenzene *via* cinnamaldehyde hydrogenation on Au/TiO<sub>2</sub> catalysts.<sup>52</sup> However, there had been no follow-up studies reported until our work.

Besides symmetrical ether production, we also observed that unsymmetrical ethers can be generated *via* a coupling reaction of two aldehydes, or an aldehyde and an alcohol, with different carbon chain lengths, as shown in Fig. 4. For example, ethyl propyl ether ( $\text{CH}_3\text{CH}_2\text{OCH}_2\text{CH}_2\text{CH}_3$ ) can be produced by acetaldehyde + propionaldehyde, ethanol + propionaldehyde, or 1-propanol + acetaldehyde on H covered Au(111). Thus, tuning the structure of precursor aldehydes and alcohols leads to the synthesis of the corresponding unsymmetrical ethers.

A reaction mechanism (Fig. 4) is proposed for this reaction. Path 1 indicates a reaction mechanism for ether synthesis *via* aldehyde-aldehyde coupling. Step (a) shows that aldehydes adsorb on the surface with a configuration of  $\eta^1(\text{O})$ .<sup>50</sup> Based on the DFT calculations used in Fig. 3b, H atoms attack the oxygen first and create an alcohol-like intermediate on the surface as step (b) shows. Subsequently, this intermediate couples with another aldehyde molecule and continues to be hydrogenated, producing the ether and water as shown in step (c)–(f). In this process, we believe that aldehyde and H both are indispensable. This is supported by three control experiments, none of which yielded ether production: (1) co-adsorption of alcohol and aldehyde on Au(111) without H; (2) aldehyde alone on Au(111) without H; and (3) alcohol and hydrogen on

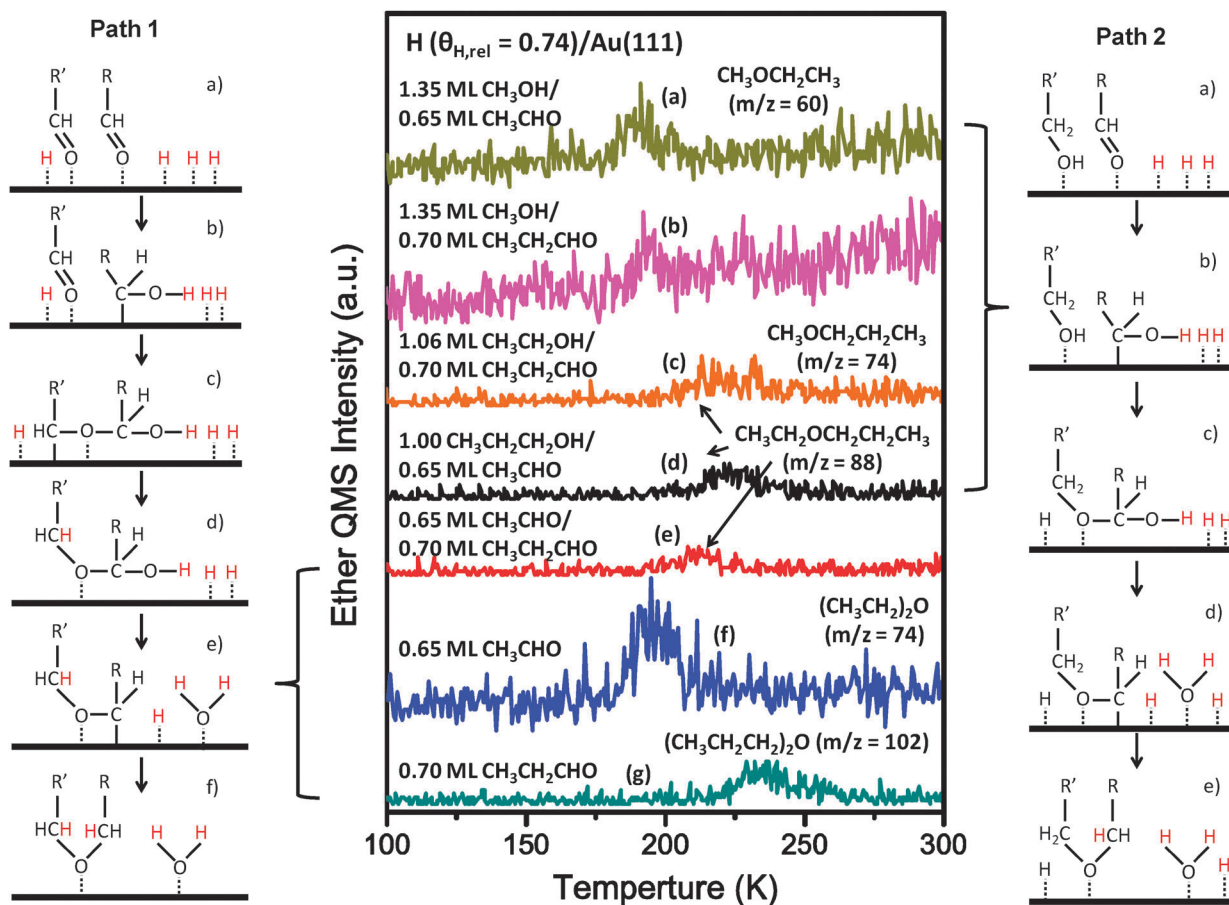


**Fig. 4** TPD spectra of produced ethers from the aldehyde-aldehyde and aldehyde-alcohol co-adsorbed Au(111) surface which is pre-covered by H atoms. Path 1 demonstrates the production of ether from aldehydes coupling. Path 2 indicates the coupling reaction between alcohols and aldehydes. When  $\text{R}' = \text{R}$ , the product is symmetrical ether. Otherwise, unsymmetrical ether is produced.<sup>12</sup> All figures obtained with permission. Copyright (2012) American Chemical Society.



Au(111). For both self-coupling reactions of acetaldehyde and propionaldehyde on H/Au(111), we found that increasing surface H coverages can reduce the selectivity of ether production compared to hydrogenation to alcohol. Based on our proposed mechanism in Path 1, the alcohol-like species formed by the partial hydrogenation of aldehyde is favorably produced with low coverage of H, leading to a high selectivity for ether production. Otherwise, higher coverages of H can promote the full hydrogenation of the aldehyde and generate alcohol on the surface, which cannot directly participate in a coupling reaction with aldehyde to produce the ether after surface H is consumed. Path 2 illustrates the coupling reaction between an aldehyde and alcohol for ether production. This process is very similar to Path 1, with the only difference being that the alcohol-like intermediate couples with an alcohol molecule [step (c)].

### 3.3 OH group interaction with H on Au(111)

Supported gold nanoparticles have been found to exhibit catalytic activity for reactions involving H and species containing an O–H group, such as water and alcohols. Studying the interaction of H–water or H–alcohol on the model Au(111) surface is useful for better understanding the mechanisms associated with these reactions.

**3.3.1. Interaction of water with H.** A fundamental understanding of the water–H interaction on gold is important to catalysis and electrochemistry. This kind of study can also provide insights into formation of hydronium ( $\text{H}_3\text{O}^+$ )<sup>53</sup> and protonated water clusters  $[(\text{H}_2\text{O})_n\text{H}^+]^{54}$  that are associated with proton transfer and transport in water, an important aspect in chemistry and biology.

It is well known that water adsorbs intact on Au(111),<sup>55</sup> exhibiting a single desorption peak at 157 K as shown in Fig. 5b. However, our study indicates that co-adsorbed H atoms can induce water dissociation.<sup>16</sup> Fig. 5c shows that when water and H atoms are co-adsorbed on the Au(111) surface,  $\text{H}_2$  TPD spectra yield two new features ( $\beta$  and  $\gamma$ ) at higher temperatures and the surface-H recombinative desorption feature (peak  $\alpha$ ) shifts from 110 K (see Fig. 5a) to 136 K. In addition, water has a higher temperature desorption feature at 175 K. By coadsorbing isotopically labeled water ( $\text{D}_2\text{O}$ ) with H atoms, as shown in Fig. 5d, the emergence of a H–D and a D–D feature, as well as a HDO feature, demonstrate that O–H bond breakage and a hydrogen exchange reaction has occurred. Further, this study and other isotope studies demonstrate that the origin of a hydrogen, either from the surface, denoted  $\text{H}_s$ , or from the water, denoted  $\text{H}_w$ , determines the desorption temperature of the  $\text{H}_2$  species, with  $\text{H}_2$  molecules containing at least one  $\text{H}_w$  when forming the 175 K  $\gamma$  feature.

DFT calculations predict, as illustrated in Fig. 6, that water clustering is a key step in the hydrogen exchange reaction.<sup>16</sup> H atoms favor adsorbing on the edge sites of the clusters, causing an “original” O–H bond to dissociate during the decomposition of water clusters that contain an extra hydrogen atom. The shift of the  $\alpha$  peak in the  $\text{H}_2$  desorption spectrum is due to a longer diffusion distance for surface H atoms, which

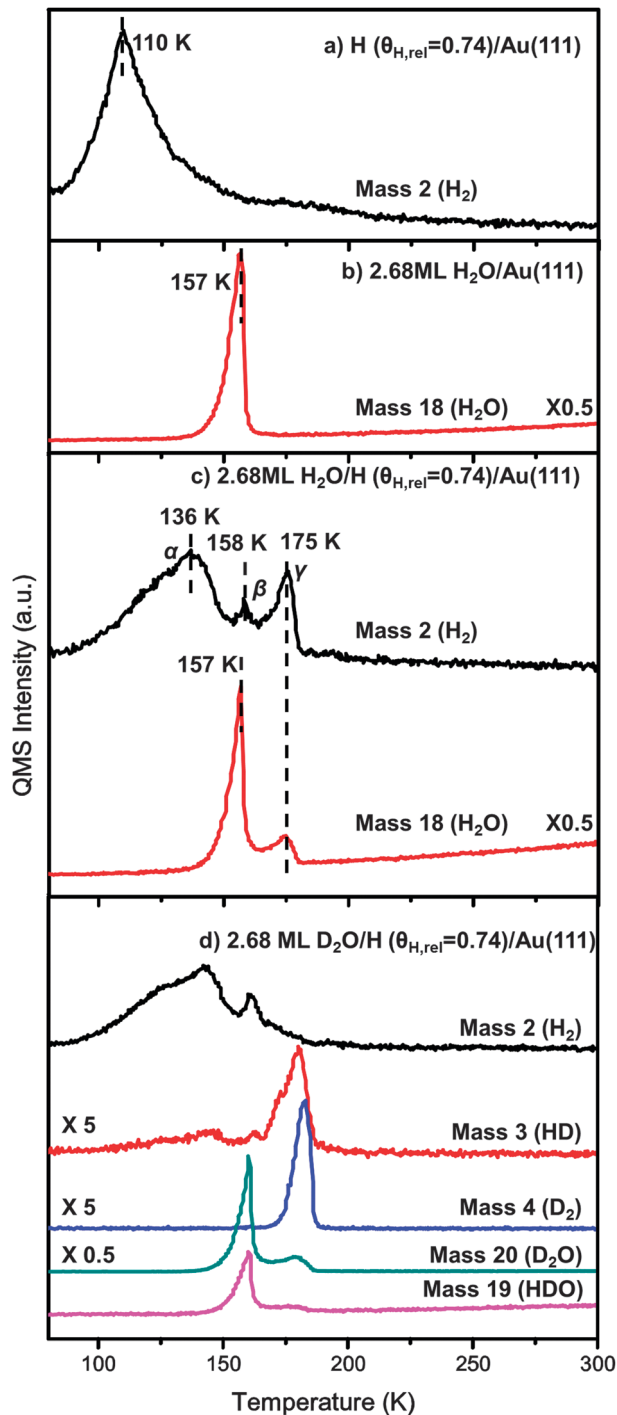


**Fig. 5** (a)  $\text{H}_2$  desorption from clean Au(111). (b) Water desorption from clean Au(111). (c) The interaction of H and  $\text{H}_2\text{O}$  on Au(111). (d) The interaction of H and  $\text{D}_2\text{O}$  on Au(111).<sup>16</sup> All figures obtained with permission. Copyright (2012) American Chemical Society.

are blocked by water clusters on the surface. Fig. 6a shows that for a single water molecule, there is a barrier of 0.29 eV for formation of hydronium ( $\text{H}_3\text{O}^+$ ), which has three equivalent O–H bonds and a small reverse barrier. This result suggests we should observe random isotopic scrambling at low temperatures, which nonetheless has not been observed with TPD.

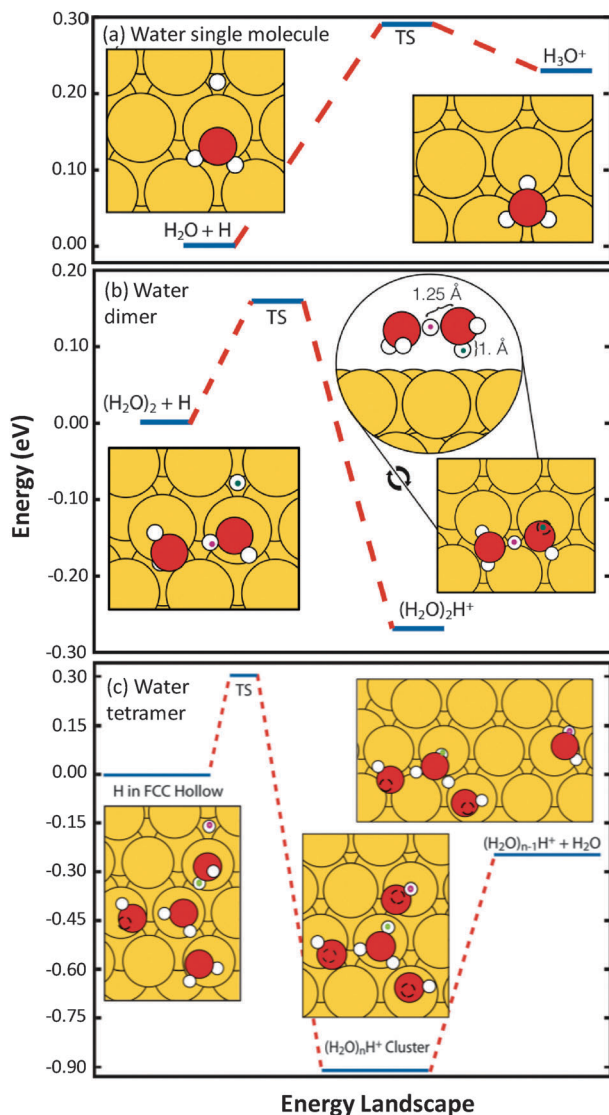


**Fig. 6** Schematic energy diagram of the interaction of atomic H with (a) a water molecule, (b) a dimer, or (c) a tetramer on Au(111).<sup>16</sup> All figures obtained with permission. Copyright (2012) American Chemical Society.

Thus, we speculate that water molecules cluster before the reaction with surface H atoms. Fig. 6b depicts the interaction of a water dimer, hydrogen bonded together, with a surface hydrogen adatom ( $H_s$ ). When the water dimer is hydrogenated, the hydrogen shared between the two water molecules (a  $H_w$ ) now has two equivalent bond lengths. This original O– $H_w$  bond in the hydrogenated water molecule is now lengthened and weaker, eventually dissociating upon heating the sample surface.

Fig. 6c illustrates the hydrogenation of a water tetramer, as a representative of a water cluster. In this example, all three edge water molecules are equally likely to desorb. However, for a larger water cluster, the two edge molecules without the bound  $H_s$  could be considered as H-bonded to other water molecules and would be unable to separate from the cluster. Thus, heating the surface results in the hydrogenated edge molecule

being the most energetic and favored to dissociate first as the cluster breaks apart. DFT calculations predict that higher energy is required to break up  $(H_2O)_nH^+$  clusters compared to  $(H_2O)_m$ , inducing a high temperature desorption feature for water at 175 K. This process ultimately causes the original O–H (or O–D) bond cleavage, leading to the isotopic H/D scrambling between water and surface atoms as well as the  $\gamma$  desorption feature as shown in Fig. 5c. In addition, the  $\beta$  peak is likely due to a physicochemical process, in which surface H atoms are physically covered by water clusters and able to leave the surface once water desorbs, showing a slightly higher desorption temperature (158 K) than the desorption of the majority water at 157 K.

**3.3.2. Interaction of H with alcohols.** In a similar study to the  $H_2O/H/Au(111)$  study, methanol and ethanol were each coadsorbed with hydrogen on a Au(111) sample.<sup>21</sup> In addition to providing a deeper insight into the interactions between the O–H functional group and hydrogen on the Au(111) surface, there are several reactions where this mechanistic information is valuable. For example, the decomposition of methanol and ethanol over supported gold nanoparticles to produce hydrogen has been previously studied, yet the interactions between reactant alcohol and produced hydrogen are not understood. In addition, as mentioned earlier, aldehydes and alcohols on a H-covered Au(111) surface can couple to produce asymmetrical ethers, with a key step requiring the dissociation of the alcohol O–H bond.<sup>12</sup>

Fig. 7 depicts the  $m/z = 2$  (H–H), 3 (H–D), and 4 (D–D) spectra for MeOH/H/Au(111) (Fig. 7a) and MeOH/D/Au(111) (Fig. 7b).<sup>17</sup> Notice that these spectra show several similarities between this system and the water and hydrogen system discussed previously: (1) both the hydrogen and the methanol–ethanol (not shown) desorption spectra show new, higher temperature features, *i.e.*, the “tail” from 150 K–210 K; (2) there is evidence of hydrogen exchange in the MeOH/D/Au(111) spectra, as indicated by the presence of H–D ( $\beta_2$ ) and H–H ( $\beta_3$ ) features; and (3) the hydrogen atoms originating from the alcohol ( $H_a$ ) desorb at higher temperatures than the hydrogen atoms originally adsorbed to the surface ( $H_s$ ). Additionally, if the H–H (mass 2), H–D (mass 3), and D–D (mass 4) spectra in Fig. 7b (MeOH/D/Au(111)) are simply added together, the composite spectrum, labeled “Masses 2 + 3 + 4”, results and although this composite spectra cannot be analyzed quantitatively, the striking similarity between the “Masses 2 + 3 + 4” spectrum in Fig. 7b and the  $m/z = 2$  spectrum in Fig. 7a gives qualitative evidence that the phenomena behind the  $\beta_1$ ,  $\beta_2$ , and  $\beta_3$  features in the MeOH–D–Au(111) system are also responsible for the “tail” feature in the MeOH–H–Au(111) system.

Overall, this stratification of hydrogen desorption features based on the origin of the hydrogen (from the surface,  $H_s$ , or from the alcohol O–H group,  $H_a$ ), combined with other observations, allowed us to propose a mechanism for this hydrogen exchange reaction based on the mechanism determined in the  $H_2O-H-Au(111)$  system: a surface hydrogen adatom,  $H_s$ , binds to a methanol molecule on the edge of a hydrogen-bonded network (dimer or larger cluster of methanol) on the Au(111)

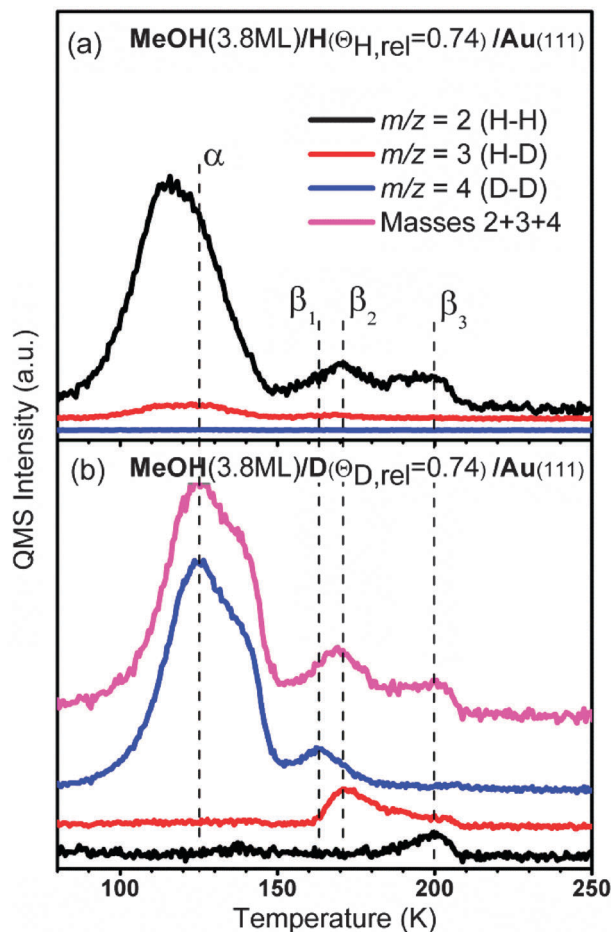


**Fig. 7** Interaction of methanol with (a) H and (b) D atoms on Au(111). "Masses 2 + 3 + 4" is the composite spectrum of adding the signals of  $m/z = 2, 3,$  and  $4$  together from 7b.<sup>17</sup> All figures obtained with permission. Copyright (2012) American Chemical Society.

surface. This methanol molecule then breaks off of the cluster, forming a  $\text{MeOH}_s$  molecule (detected in isotope experiments), and leaves its original hydroxyl hydrogen,  $\text{H}_a$ , bound to the edge of the methanol network. As the system is heated, the methanol molecules and hydrogen adatoms that were not interacting with each other desorb first. Then, methanol molecules and  $\text{H}_s$  adatoms that were interacting with each other on the surface, but did not undergo a hydrogen exchange reaction, desorb, forming the  $\beta_1$   $\text{H}_s$ - $\text{H}_s$  feature, and a corresponding methanol desorption feature. With increasing temperature, the dimers and small clusters containing an extra  $\text{H}_a$  atom start to break apart, allowing the methanol molecules to desorb and leaving a  $\text{H}_a$  atom on the surface. At lower temperatures, a few  $\text{H}_s$  adatoms are still bound to the surface, allowing the formation of the  $\text{H}_a$ - $\text{H}_s$  ( $\beta_2$ ) feature. However, at higher temperatures, only  $\text{H}_a$  atoms remain, permitting  $\text{H}_a$ - $\text{H}_a$  to be formed ( $\beta_3$  feature).

## 4. Conclusions

Gold-based catalysts have been studied for many hydrogenation reactions, showing remarkable activities, particularly for

selective transformations. However, the related fundamental studies on model gold surfaces are lacking and highly desired in order to provide reaction mechanisms. This review summarizes our recent work on hydrogenation reactions on a Au(111) single crystal surface using atomic hydrogen to pre-populate the surface. These studies aim to understand the role of gold in hydrogenation reactions after dissociated H atoms diffuse onto the gold surface, and further provide insight into the catalytic properties of classical supported gold nanoparticle catalysts. Our model studies show the following interesting experimental results:

(i) Hydrogen adatoms weakly bind on Au(111) with a desorption peak at 110 K, indicating an activation energy for recombinative desorption of  $\sim 28 \text{ kJ mol}^{-1}$ .

(ii) The reduction of nitrogen dioxide occurs at 77 K on H/Au(111), yielding a high  $\text{NO}_2$  conversion (100%) and NO selectivity (100%) upon heating the surface to  $\sim 120 \text{ K}$ .  $\text{HNO}_2$  and  $\text{N}_2\text{O}_3$  are the likely reaction intermediates.

(iii) Acetaldehyde can be hydrogenated to ethanol on H-pre-covered Au(111). The Au(111) surface also shows activity for propionaldehyde hydrogenation to 1-propanol but not for acetone hydrogenation to 2-propanol. This difference is likely due to dissimilarities in the energetic barriers of the reaction steps and that polymerization of propionaldehyde allows the molecules to remain on the surface at higher temperatures, increasing the reaction probability.

(iv) Ethers can be synthesized *via* a coupling reaction of aldehydes or aldehyde-alcohol on H/Au(111), where the alcohol-like intermediate from the partial hydrogenation of aldehydes likely plays a key role for the production of ethers.

(v) Water and alcohols have a strong interaction with H on Au(111) and show H/D exchange in isotopic experiments, indicating dissociation of the O-H group. The isotopic experiments also help to identify the sources of desorption features of  $\text{H}_2$  (from surface H atoms or H in water-alcohols), allowing for speculation of a reaction mechanism.

In summary, the model gold surface, Au(111), shows a unique catalytic activity for selective hydrogenation reactions. Weakly bound H atoms demonstrate reactivity for hydrogenation reactions and can yield a high selectivity for partially hydrogenated products. The aim of this work was to provide additional mechanistic information for gold catalytic activity for hydrogenation reactions and enhance the understanding of hydrogenation chemistry of classical supported gold catalysts at the molecular scale.

## Acknowledgements

We acknowledge the generous support of the Department of Energy (DE-FG02-04ER15587) and the Welch Foundation (F-1436 for C.B.M., F-1601 for G.H., and F-1535 for G.S.H.). Ming Pan acknowledges the William S. Livingston Fellowship for financial support. Zachary D. Pozun acknowledges support through the Dorothy B. Banks Fellowship and NSF grant no.OCI-1225384.

## Notes and references

- 1 M. Haruta, T. Kobayashi, H. Sano and N. Yamada, *Chem. Lett.*, 1987, 405–408.
- 2 A. S. K. Hashmi and G. J. Hutchings, *Angew. Chem., Int. Ed.*, 2006, **45**, 7896–7936.
- 3 B. K. Min and C. M. Friend, *Chem. Rev.*, 2007, **107**, 2709–2724.
- 4 R. Meyer, C. Lemire, S. Shaikhtudinov and H. Freund, *Gold Bull.*, 2004, **37**, 72–124.
- 5 T. Janssens, B. Clausen, B. Hvolbæk, H. Falsig, C. Christensen, T. Bligaard and J. Nørskov, *Top. Catal.*, 2007, **44**, 15–26.
- 6 G. C. Bond, P. A. Sermon, G. Webb, D. A. Buchanan and P. B. Wells, *J. Chem. Soc., Chem. Commun.*, 1973, 444–445.
- 7 G. J. Hutchings, *J. Catal.*, 1985, **96**, 292–295.
- 8 P. Claus, *Appl. Catal., A*, 2005, **291**, 222–229.
- 9 M. Haruta and M. Date, *Appl. Catal., A*, 2001, **222**, 427–437.
- 10 T. Fujitani, I. Nakamura, T. Akita, M. Okumura and M. Haruta, *Angew. Chem., Int. Ed.*, 2009, **48**, 9515–9518.
- 11 A. G. Sault, R. J. Madix and C. T. Campbell, *Surf. Sci.*, 1986, **169**, 347–356.
- 12 M. Pan, A. J. Brush, G. Dong and C. B. Mullins, *J. Phys. Chem. Lett.*, 2012, **3**, 2512–2516.
- 13 M. Pan, D. W. Flaherty and C. B. Mullins, *J. Phys. Chem. Lett.*, 2011, 1363–1367.
- 14 M. Pan, H. C. Ham, W.-Y. Yu, G. S. Hwang and C. B. Mullins, *J. Am. Chem. Soc.*, 2013, **135**, 436–442.
- 15 M. Pan, Z. D. Pozun, A. J. Brush, G. Henkelman and C. B. Mullins, *ChemCatChem*, 2012, **4**, 1241–1244.
- 16 M. Pan, Z. D. Pozun, W.-Y. Yu, G. Henkelman and C. B. Mullins, *J. Phys. Chem. Lett.*, 2012, **3**, 1894–1899.
- 17 A. J. Brush, M. Pan and C. B. Mullins, *J. Phys. Chem. C*, 2012, **116**, 20982–20989.
- 18 H. Sakurai and M. Haruta, *Appl. Catal., A*, 1995, **127**, 93–105.
- 19 H. Sakurai, S. Tsubota and M. Haruta, *Appl. Catal., A*, 1993, **102**, 125–136.
- 20 A. Hugon, L. Delannoy and C. Louis, *Gold Bull.*, 2008, **41**, 127–138.
- 21 S. Galvagno, J. Schwank and G. Parravano, *J. Catal.*, 1980, **61**, 223–231.
- 22 Y. Azizi, C. Petit and V. Pitchon, *J. Catal.*, 2008, **256**, 338–344.
- 23 M. Boronat, P. Concepcin, A. Corma, S. Gonzalez, F. Illas and P. Serna, *J. Am. Chem. Soc.*, 2007, **129**, 16230–16237.
- 24 B. Campo, C. Petit and M. A. Volpe, *J. Catal.*, 2008, **254**, 71–78.
- 25 T. V. Choudhary, C. Sivadinarayana, A. K. Datye, D. Kumar and D. W. Goodman, *Catal. Lett.*, 2003, **86**, 1–8.
- 26 C. Mohr, H. Hofmeister, J. Radnik and P. Claus, *J. Am. Chem. Soc.*, 2003, **125**, 1905–1911.
- 27 A. Corma and H. Garcia, *Chem. Soc. Rev.*, 2008, **37**, 2096–2126.
- 28 B. Xu, X. Liu, J. Haubrich and C. M. Friend, *Nat. Chem.*, 2010, **2**, 61–65.
- 29 B. Hammer and J. K. Norskov, *Nature*, 1995, **376**, 238–240.
- 30 I. Nakamura, H. Mantoku, T. Furukawa and T. Fujitani, *J. Phys. Chem. C*, 2011, **115**, 16074–16080.
- 31 D. A. Panayotov, S. P. Burrows, J. T. Yates and J. R. Morris, *J. Phys. Chem. C*, 2011, **115**, 22400–22408.
- 32 M. Bron, E. Kondratenko, A. Trunschke and P. Claus, *Z. Phys. Chem.*, 2004, **218**, 405–424.
- 33 J. Greeley and M. Mavrikakis, *J. Phys. Chem. B*, 2005, **109**, 3460–3471.
- 34 D. Kolovos-Vellianitis and J. Küppers, *Surf. Sci.*, 2004, **548**, 67–74.
- 35 H. L. Tierney, A. E. Baber, J. R. Kitchin and E. C. H. Sykes, *Phys. Rev. Lett.*, 2009, **103**, 246102.
- 36 E. Bus, J. T. Miller and J. A. van Bokhoven, *J. Phys. Chem. B*, 2005, **109**, 14581–14587.
- 37 K. Burke and A. Hodgson, *Surf. Sci.*, 2004, **566–568**, 186–191.
- 38 J. Boh, G. Eilmsteiner, K. D. Rendulic and A. Winkler, *Surf. Sci.*, 1998, **395**, 98–110.
- 39 K. Christmann, O. Schober, G. Ertl and M. Neumann, *J. Chem. Phys.*, 1974, **60**, 4528–4540.
- 40 A. Tamtogl, M. Kratzer, J. Killman and A. Winkler, *J. Chem. Phys.*, 2008, **129**, 224706–224708.
- 41 J. R. Engstrom, W. Tsai and W. H. Weinberg, *J. Chem. Phys.*, 1987, **87**, 3104–3119.
- 42 D. E. Ibbotson, T. S. Wittrig and W. H. Weinberg, *J. Chem. Phys.*, 1980, **72**, 4885–4895.
- 43 S. C. Gebhard and B. E. Koel, *J. Phys. Chem.*, 1992, **96**, 7056–7063.
- 44 K. L. Kostov, W. Widdra and D. Menzel, *Surf. Sci.*, 2004, **560**, 130–144.
- 45 I. N. Yakovkin, V. D. Osovskii, N. V. Petrova and Y. G. Ptushinskii, *Surf. Rev. Lett.*, 2006, **13**, 375–386.
- 46 T. U. Nahm and R. Gomer, *Surf. Sci.*, 1997, **375**, 281–292.
- 47 A. Hodgson, A. Wight, G. Worthy, D. Butler and B. E. Hayden, *Faraday Discuss.*, 1993, **96**, 161–173.
- 48 M. Gomez-Gallego and M. A. Sierra, *Chem. Rev.*, 2011, **111**, 4857–4963.
- 49 T. M. Salama, R. Ohnishi, T. Shido and M. Ichikawa, *J. Catal.*, 1996, **162**, 169–178.
- 50 D. Syomin and B. E. Koel, *Surf. Sci.*, 2002, **498**, 53–60.
- 51 K. P. C. Vollhardt and N. E. Schore, *Organic Chemistry – Structure and Function*, W. H. Freeman and Company, New York, 4th edn, 2002.
- 52 C. Milone, M. C. Trapani and S. Galvagno, *Appl. Catal., A*, 2008, **337**, 163–167.
- 53 F. T. Wagner and T. E. Moylan, *Surf. Sci.*, 1988, **206**, 187–202.
- 54 J. W. Shin, N. I. Hammer, E. G. Diken, M. A. Johnson, R. S. Walters, T. D. Jaeger, M. A. Duncan, R. A. Christie and K. D. Jordan, *Science*, 2004, **304**, 1137–1140.
- 55 R. A. Ojifinni, N. S. Froemming, J. Gong, M. Pan, T. S. Kim, J. M. White, G. Henkelman and C. B. Mullins, *J. Am. Chem. Soc.*, 2008, **130**, 6801–6812.